

Galaxy Zoo Hubble: the evolution of red disk galaxies since $z = 1$

Melanie A. Galloway¹

¹*School of Physics and Astronomy, University of Minnesota, 116 Church St. SE, Minneapolis, MN 55455, USA*

10 October 2017

ABSTRACT

We study the evolution of the passive disk population from $z = 1$ to $z = 0.3$ in a sample of 14,000 galaxies from the COSMOS field and morphologically classified by the Galaxy Zoo: Hubble project. We find the fraction of disks occupying the red sequence, as well as the fraction of disk galaxies that are red, to decrease for the most massive galaxies ($\log(M/M_\odot) > 11$) but increase for lower masses. We interpret the trends in these fractions by identifying four dominant drivers of the change in numbers for each population: the rate of blue disks quenching to become red disks, the rate of red disks transforming to red ellipticals, the rate of blue disks quenching while morphologically transforming to red ellipticals, and the net elliptical merger rate. We develop a toy model to simulate the evolution of the passive disk fractions using a range of input rate parameters. Using the best-fit results of the model, we estimate that $20 \pm \text{error} \%$ of massive galaxies go through a passive disk phase, and this fraction decreases with mass. This paper also introduces a new method for using artificially-redshifted galaxies to quantify the redshift-bias in Galaxy Zoo classifications in order to accurately measure the fraction of disk galaxies as a function of redshift.

1 INTRODUCTION

Passive, red disks are an unconventional class of galaxies. They do not adhere to the standard bimodality of the color-morphology relationship, whereby most galaxies tend to exist in one of two populations: blue, late-type disks exhibiting active star formation, and red, early-type ellipticals showing little to no signs of recent star formation (Strateva et al. 2001; Baldry et al. 2004; Correa et al. 2017). The division between the two populations is particularly apparent when represented visually on a color-magnitude or color color diagram. Galaxies tend to populate in two distinct regions: the “red sequence” in the upper band, which contains predominantly early-type galaxies, and the “blue cloud” in the lower, containing mostly late-type spirals. This relationship has been shown to hold for $\sim 85\%$ of galaxies out to $z \sim 1$ (Bell et al. 2004; Cirasuolo et al. 2007; Mignoli et al. 2009) and possibly beyond (Giallongo et al. 2005; van Dokkum et al. 2006; Franzetti et al. 2007; Cassata et al. 2008).

The relatively tight correlation between galaxy color (which traces the stellar content) and morphology (which traces dynamical history) suggests an evolutionary link between the two. In the simplest interpretation, it could be deduced that galaxies tend to begin their lives as young, star-forming disks, until some mechanism (secular or external) causes star-formation to cease while the galaxy simultaneously undergoes a morphological transformation from disk to spheroidal. The growing evidence for a significant population of galaxies which breaks this relationship, however, insists on more nuanced interpretations of this model.

The passive disk population has been a matter of interest for understanding the mechanisms driving the evolutionary link between color and morphology since their initial discovery. In one of the earliest documented reports of this class, van den Bergh (1976) identified a set of spirals in the Virgo cluster which were forming stars “much less vigorously” than the other galaxies of the same type, which were dubbed “anemic spirals”. Analysis of this population suggested the possibility of “gentle” quenching mechanisms which could shut off star-formation without disrupting the morphology (in contrast to violent processes such as mergers, which are capable of destroying the disk (Bell et al. 2004; Negroponte & White 1983; De Lucia et al. 2006; Springel et al. 2005)). The low gas content in the anemic spirals suggested that subtle environmental factors played a role in stripping the gas required to continue star-formation, a process commonly known now as ram-pressure stripping (Gunn & E. and Gott, III 1972; Steinhauser et al. 2016).

Other studies have since investigated other possible mechanisms could lead to the formation of passive disks, and how significant of a contribution this population makes to understanding the full picture of galaxy evolution. Environment is believed to play a strong role in thier formation; many studies for instance find passive spirals preferentially in high-density environments (Dressler et al. 1999; Poggianti et al. 1999; Goto et al. 2003; Deng et al. 2009; Hughes & Cortese 2009). Moran et al. (2006) model the star-formation histories of passive spirals at $z \sim 0.4$ and find them to be consistent with models for spirals affected by gas-starvation

(Larson, R.B., Tinsley, B.M. and Caldwell 1980; Quilis et al. 2000; Bekki et al. 2002). Environment plays a significant factor in this scenario, whereby the interaction of the galaxy with the intra-cluster medium halts the accretion of gas onto the galaxy, inhibiting star-formation and causing a quench without disrupting the morphology significantly. Their results did not argue that starvation was the only mechanism responsible for building up the population of disks in the red sequence, but do conclude that passive disks are indeed an important transition population.

Masters et al. (2010) is one of the few studies which finds no strong correlation of passive disks with environment, but do not rule out environment playing a significant contribution in their creation. They also find strong evidence for quenching via completely secular processes; given by their sample of passive disks being more massive and having a higher bar fraction than their star-forming counterparts. Massive galaxies are more likely to have been assembling for very long times, allowing sufficient time to use up all of their gas, without environment being a direct factor. This option could explain the observed correlations with density and passivity, given that higher-density regions were more likely to have been assembled at earlier times. Secondly, Masters et al. (2010) observed a significantly higher bar fraction in passive spirals (67%) than star-forming spirals (27%). Bars are known for their ability to efficiently drive gas to the centers of galaxies via a redistribution of angular momentum throughout the disk (Sellwood & Wilkinson 1993; Shlosman et al. 1989; Ann & Thakur 2005), which could increase central star-formation (Hawarden et al. 1986; Ho et al. 1997) or feed the central supermassive black hole (Athanasoula 1992; Friedli & Benz 1993). The excess of bars in passive disks then suggests that bars were responsible for quickly using up the gas in the galaxy, resulting in subsequent quenching.

Passive disks have thus far been proposed as both a final stage of galactic evolution, driven by secular and external processes capable of exhausting gas required for star-formation, and as a transition phase of galaxies toward a final evolution to red spheroidal, driven by processes which quench and morphologically transform on different timescales, or multiple separate processes acting independently. Understanding the significance of the passive disk population is therefore unquestionably an important key to understanding galaxy evolution as a whole. Bundy et al. (2010) investigates this subject by measuring the different morphological contributions to the red sequence since $z = 1$, and estimate as high as 60% of all galaxies go through a passive disk phase. It was not quantified which of these further evolve to spheroidal and which stay disks for the remainder of their lifetimes, but the decaying contribution of passive disks to $z = 0.3$ was evidence that some fraction of these did indeed transform to elliptical.

This paper will investigate the evolution of the passive disk population from $z = 1$ to $z = 0.3$ using galaxies identified in the COSMOS field with morphological classifications from Galaxy Zoo: Hubble. We will measure the fraction of disks which are passive and the fraction of the red sequence occupied by disks as functions of mass and redshift, and argue that three factors drive the evolution of these fractions: 1) the rate of blue disks quenching to form passive disks, 2) the rate of blue disks quenching and simultaneously trans-

forming to elliptical, 3) the rate of red disks transforming to red ellipticals, and 4) the net merger rate of ellipticals. We will implement a simple toy model to simulate the evolution of the relative abundances of red disks, blue disks, and red ellipticals, in order to quantify these rate parameters. We will use the results to estimate the fraction of galaxies that enter a red disk phase, and discuss the likelihoods of the red disk phase being a transitory stage or an end-point of a typical galaxy’s evolutionary path.

Section 2 will describe our methods for selecting disk galaxies and separating the sample into active / passive populations using a color-color diagnostic. In Section 3 we describe a new method of correcting for redshift bias in the detection of disk galaxies with Galaxy Zoo classifications using an artificially-redshifted set of images. In Section 4 we present our results of the fraction of disk galaxies which are red, and the fraction of red sequence galaxies that are disks, as functions of mass and redshift. Here we also explain our toy-model for measuring the dominant evolutionary pathways taken by galaxies in different bins of mass. We compare our findings with results from the literature and discuss their implications in Section ???. Our main conclusions are outlined in Section 6. We adopt a Λ CDM cosmology throughout this paper of $\Omega_m = 0.31$ and $H_0 = 68 \text{ km s}^{-1} \text{ Mpc}^{-1}$ (Planck Collaboration et al. 2015).

2 DATA

The parent sample of galaxies in this paper is drawn from the Galaxy Zoo: Hubble (GZH) catalog (Willett et al. 2016), which provides morphological classifications for galaxies sourced from the HST Legacy Surveys. From the main catalog we select galaxies with imaging from the Cosmic Evolution Survey (COSMOS, Scoville et al. (2007)) in the redshift range $0 < z < 1$. Rest frame NUV-r and r-J colors are taken from the UltraVISTA catalog (McCracken et al. 2012; Ilbert et al. 2013).

2.1 Sample Selection

We identify a sample of 14,663 disk and elliptical galaxies using the morphological classifications provided by GZH. Mergers and irregulars are excluded from the analysis by applying cuts of $f_{\text{irregular}} > 0.3$ and $f_{\text{merger}} > 0.5$ for galaxies which have at least 20 “yes” votes for the question, “Is there anything odd?”. Last, we apply an inclination limit using $f_{\text{not edge-on}} > 0.3$ and $N_{\text{not edge-on}} > 10$. Before applying this cut, it was observed that the red sequence region of the sample was dominated by highly-inclined galaxies, shown in Figure 1. Given that galaxy color should be independent of the angle in which it is observed, it is clear that the inclined galaxy colors are strongly affected by dust-reddening. While we are not using dust-corrected colors in our color-color separation, inclination has shown to have an affect on colors even in those which dust-corrected has been attempted (Morselli et al. 2016; Devour & Bell 2017). By limiting the sample to face-on galaxies, this bias should be removed (right panel of Figure 1).

To classify the galaxies as quiescent or star-forming, a method similar to that described by Ilbert et al. (2013) (hereafter I13) was used, which implements a rest-frame

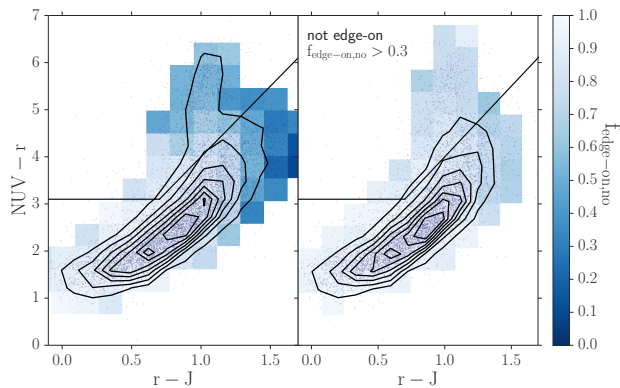


Figure 1. The effect of reddening for highly inclined galaxies. On the left panel is the distribution of $f_{\text{edge-on,no}}$, which is the fraction of Galaxy Zoo users who voted “no” in response to the question “Could this be a galaxy viewed edge-on?”. This vote correlates with inclination angle, such that low values represent highly inclined galaxies, and high values represent face-on galaxies. The bins are colored such that darker blue bins have a higher fraction of highly inclined galaxies, and white bins have high fractions of face-on galaxies. There is an obvious bias towards redder colors for galaxies with high inclination angles (low votes for $f_{\text{edge-on,no}}$). We therefore implement a cut of $f_{\text{edge-on,no}} > 0.3$ to ensure that observed red colors are an indicator of a lack of star-formation, and not dust-reddening. [Note: I’m not sure the right panel is particularly useful; it’s really just showing the distribution is mostly smoothed out after setting the cut. Keep?]

NUV- r versus r - J diagnostic. Here are some reasons these colors are great (NUV- r): (Arnouts et al. 2007; Salim et al. 2005; Wyder et al. 2007), (Martin et al. 2007)

The demarcation line to separate the quiescent and active populations at $z = 1$ is adopted from I13, which defines the quiescent galaxies as those which satisfy: $M_{\text{NUV}} - M_r > 3(M_r - M_J) + 1$ and $M_{\text{NUV}} - M_r > 3.1$. I13 applies this criteria to all galaxies in a range of $0.2 < z < 3$, although it performs best at separating the two populations in the redshift bin $0.7 < z < 1.2$, where $> 98\%$ of galaxies identified as quiescent exhibited star formation rates less than $\log(\text{SFR}) = -11$ (see Figure 3 of I13). Therefore this work uses the I13 separation criteria at $z = 1$, and computes the evolution of the demarcation lines as a function of redshift to $z = 0$.

The evolution of r - J and $\text{NUV} - r$ colors was measured using a stellar population synthesis model from Bruzual & Charlot (2003). An instantaneous-burst model (ssp) was chosen from the Padova1994 track to represent the color evolution of a passively evolving galaxy, with a metallicity $Z = 0.008 = .4Z_{\odot}$, which is the typical metallicity of passive galaxies with mass $9 < \log(M_*/M_{\odot}) < 10$ (Peng et al. (2015), Figure 2a), chosen to correspond to the median mass of the sample ($\log(M_*/M_{\odot}) = 9.7$). A linear fit was generated for each color within the range $0 < z < 2$, and the slopes for each were used to redefine the demarcation lines in five redshift bins: one with central value $z = 0.007$ (used to classify the SDSS ferengi2 sample), and four with central values $z = [0.30, 0.50, 0.70, 0.90]$ with widths $\Delta z = 0.2$. The quiescent galaxies are thus defined in these bins as those that satisfy:

$$M_{\text{NUV}} - M_r > 3.1 + a_1(z) \quad (1)$$

$$M_{\text{NUV}} - M_r > 3(M_r - M_J + a_2(z)) + a_1(z) + 1 \quad (2)$$

where $a_1(z) = [0.54, 0.38, 0.27, 0.16, 0.05]$ and $a_2(z) = [0.19, 0.14, 0.10, 0.06, 0.02]$.

We note that the evolution of the demarcation lines from $z = 1$ to $z \sim 0$ is very minimal, and our final results do not change if we perform the separation using static lines.

In describing our methods for separating active and passive populations using a color-color separation technique, we have used terminology such that blue/red have been used to describe colors explicitly, while active/passive have been used to describe ongoing/quenched star-formation. The remainder of this paper will assume that the color cuts described in this section adequately separated the active and passive populations, and for convenience the terms red/blue will be used interchangeably with passive/active. k thanks!

3 CORRECTING FOR INCOMPLETENESS IN DISK DETECTION

In this work, we study the growth of the red sequence population by evaluating the fraction of passive disks as a function of redshift, $N_{\text{red disks}}/(N_{\text{red disks}} + N_{\text{blue disks}})$, as well as the fraction of disks occupying the red sequence, $N_{\text{red disks}}/(N_{\text{red disks}} + N_{\text{red ellipticals}})$. To accurately measure these fractions, the number of disks populating each redshift interval must be known with confidence. To identify disk galaxies in our sample, we set a cut of $f_{\text{features}} \geq 0.3$, such that galaxies meeting this criteria are considered to have distinguishable features or disk structure (additional cuts are also placed to eliminate clumpy, highly inclined, and merging galaxies; see Section 2.1). However, it is known that distinguishing disk structure from spheroidal becomes increasingly challenging at high redshifts (for both experts and novice classifiers alike), where features are less resolved and more difficult to identify. Willett et al. (2016) show using a set of artificially-redshifted simulated galaxy images classified in Galaxy Zoo that vote fractions for the same galaxy can be drastically different measured at $z = 1$ from $z = 0$, often enough to change its morphological classification (we will show the same in Section 3.1). Therefore it is predicted that applying a f_{features} cut to identify disks will increasingly underestimate their true number at increasing redshift intervals. A set of artificially redshifted images was used to quantify and correct for this incompleteness in disk detection, described in the next section.

3.1 FERENGI2 set of artificially redshifted galaxy images

FERENGI2 is a set of simulated galaxy images created using the FERENGI code (Barden et al. 2008). These were created from a parent sample of 936 nearby ($z < 0.01$) SDSS galaxies, all of which had been previously classified in Galaxy Zoo 2 and were cross-matched in 2MASS (Skrutskie et al. 2006) for J magnitudes and GALEX (Martin et al. 2005) for

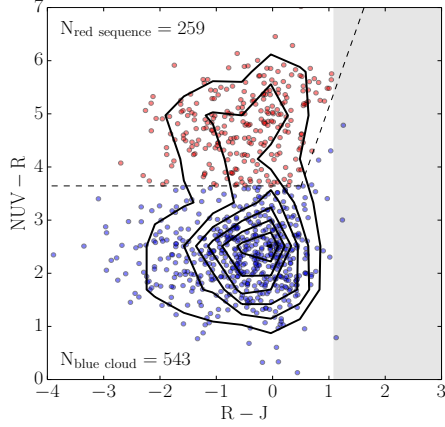


Figure 2. Separation of the quiescent population (red sequence) and active population (blue cloud) of the FERENG12 sample. The gray shaded region represents the R-J limit of the sample; since FERENG12 is a subset of GZ2, for which a limit of $r < 17$ was implemented, and the magnitude limit of 2MASS is $J < 15.91$, the FERENG12 sample is limited to $R-J < 1.1$.

NUV magnitudes, which were necessary to create a color-color separation using a method as similar as possible to that of the COSMOS sample. An evolution factor of $e = -1$ was applied, which brightens each galaxy linearly with redshift: $M' = M + ez$, where M' is the corrected magnitude. This correction is performed to mimic the known physical increase of galaxy magnitude with redshift (Lilly et al. 1998; Loveday et al. 2011), and the value $e = -1$ was chosen based on an analysis of spectra template models provided by Brinchmann et al. (2004), which showed that typical galaxies tend to evolve in brightness by one magnitude per redshift. Each galaxy was artificially redshifted 8 times from $z = 0.3$ to $z = 1$ in intervals of $\Delta z = 0.1$ and processed to mimic *HST* imaging parameters, giving a total of 7,488 images (3 examples are shown in Figure 3). The set was then classified in Galaxy Zoo using the same decision tree as used for Galaxy Zoo Hubble. 134 highly inclined disk galaxies were removed from the sample by excluding any with $N_{\text{edge-on}} > 20$ and $f_{\text{not edge-on}} \geq 0.6$, using the vote fraction associated with the real galaxy image measured in GZ2. This cut was shown in Galloway et al. (2015) to correlate well with inclination angle $\cos(a/b) < 67^\circ$. This was to exclude those which may be mis-classified due to dust-reddening. Using the NUV-J-R selection method described in section 2.1, the remaining sample was divided into a set of red sequence galaxies (259 per redshift bin) and blue cloud (543 per each redshift bin) (see Figure 2).

3.2 Measuring ξ

The FERENG12 set was used to measure the incompleteness in disk detection, from which a correction factor ξ was derived. This is defined as the number of disks detected divided by the true number of disks expected to exist in a given redshift interval: $\xi(z) = N_{\text{detected}}/N_{\text{true}}$. Acknowledging that the completeness in disk detection may depend on

galaxy color, the corrected fraction of passive disks can then be calculated as:

$$f_{R|D} = \frac{N_{RD} \times \xi_{\text{red}}^{-1}}{N_{RD} \times \xi_{\text{red}}^{-1} + N_{BD} \times \xi_{\text{blue}}^{-1}} \quad (3)$$

If there is no color bias in disk detection, $\xi_{\text{red}} = \xi_{\text{blue}}$, and this term cancels out, leaving the fraction unchanged. If there is a bias, however, the ξ terms do not cancel, and the incompleteness in disk detection could have a large effect on the red disk fraction. Therefore a careful measurement of ξ is estimated for both red and blue disk galaxies using the FERENG12 set of simulated images.

The completeness values $\xi_{\text{red}}(z)$ and $\xi_{\text{blue}}(z)$ were computed in varying bins of redshift for the red sequence and blue cloud galaxies separately. An example calculation of ξ_{blue} in the $z = 0.7$ bin is shown in Figure 4. Each point represents a FERENG12 galaxy, where the y-axis indicates the value of f_{features} measured in the image redshifted to $z = 0.7$, and the x-axis indicates the value of f_{features} measured in the same galaxy redshifted to $z = 0.3$. Disk galaxies are identified as those for which $f_{\text{features}} \geq 0.3$. Since, on average, f_{features} decreases for the same galaxy as it is viewed at higher redshifts, the number of galaxies meeting this threshold is generally fewer at higher redshifts than lower redshifts. This is indicated by the dotted lines: galaxies to the right of the vertical dashed line at $f_{\text{features}, z=0.3} = 0.3$ are identified as disks at $z = 0.3$; their sum is considered the “true” number of disks, N_{true} . Similarly, the galaxies above the horizontal line at $f_{\text{features}, z=0.7} = 0.3$ are identified as disks at $z = 0.7$; their sum is the “detected” number of disks at $z = 0.7$, or N_{detected} . As obvious in the figure, N_{detected} is in general much lower than N_{true} , emphasizing the increasing difficulty in detecting features at higher redshifts. Their ratio is the completeness ξ ; in this example $\xi_{\text{blue}}(z = 0.7) = 0.61$, meaning only 61% of disks were detected at this redshift.

It was hypothesized that the completeness in disk detection may be a function of other parameters in addition to redshift. At fixed redshift, for example, it is reasonable to guess that features could be easier to detect galaxies that have higher mass, radius, or surface brightness. To test whether these parameters also impact the number of disks detected, the completeness was measured in fixed redshift bins as a function of surface brightness, effective radius, and mass. The surface brightness was calculated as $\mu = m + 2.5 \times \log_{10}(2 \times (b/a) \times \pi R_e^2)$, using SEXTRACTOR outputs `MAG_AUTO`, `b/a` and `R_e` measured in the I_{814W} band images. The effective radius used was the 50% `FLUX_RADIUS` converted in to kpc, and the masses used were the `MEDIAN` values in the MPA-JHU DR7 catalog (Kauffmann et al. 2003).

Figure 5 shows completeness as a function of redshift and surface brightness, for the red sequence and blue cloud galaxies. 8 redshift bins were further divided into bins of surface brightness with varying widths, where the sizes were chosen to satisfy that $N_{\text{detected}} + N_{\text{true}} \geq 10$ in each bin. This was chosen as a compromise between having a sufficient number of galaxies in each bin to compute the completeness fraction $\xi = N_{\text{detected}}/N_{\text{true}}$, and to have enough bins of surface brightness to measure a trend with confidence of completeness as a function of μ . Visual inspection of the data did not suggest any relationship between the two. To be sure,

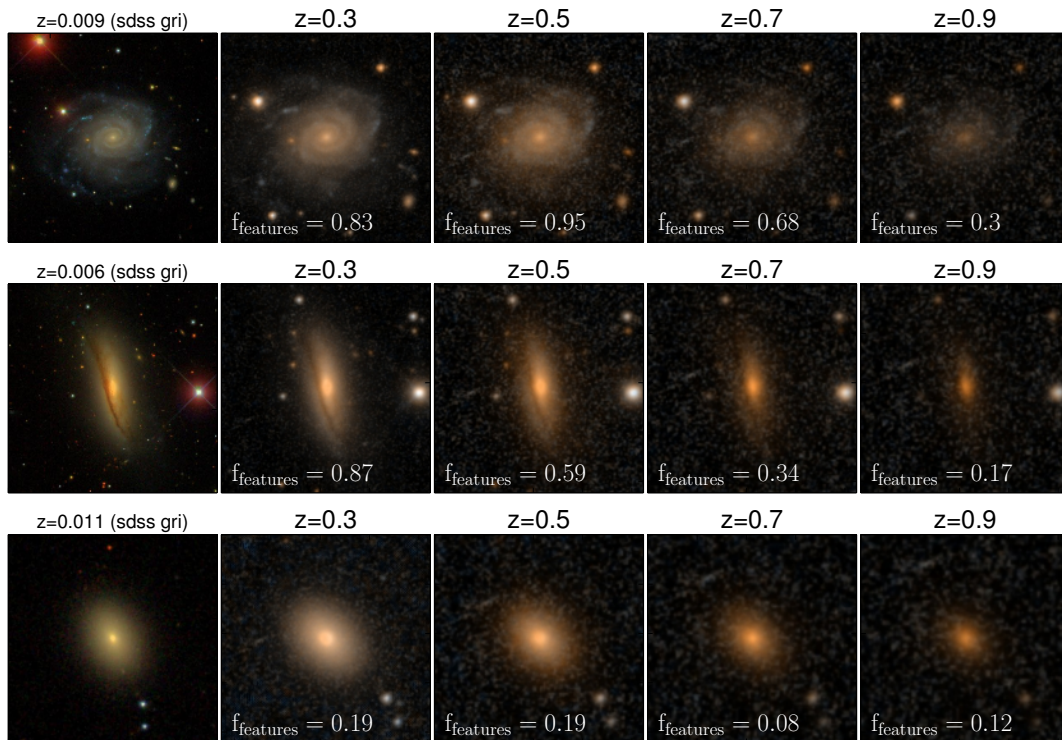


Figure 3. Example images of three galaxies artificially redshifted with the FERENGI code. The left image in each row is a real SDSS gri-composite image; the four to the right are images generated by FERENGI at varying redshifts, processed to mimic *HST/COSMOS* imaging. The f_{features} vote fraction for each simulated image is given; this value tends to decrease for each galaxy as it is processed to be viewed at higher redshifts.

the data were fit to a linear function in each redshift bin. For each fit, a p-value representing a hypothesis test whose null hypothesis is that the slope is zero was computed. Only one reached the criteria $p < 0.05$, but with a low R^2 value of 0.28 which is not considered large enough to represent a good fit. This process was repeated using effective radius and mass as parameters, with the same results. Therefore only redshift was used as a parameter which impacted completeness value with confidence.

The completeness values ξ_{red} and ξ_{blue} were then measured as a function of redshift for the red sequence and blue cloud FERENGI2 galaxies; results are shown in Figure 6. No significant difference was detected for the two functions, which is apparent from the overlapping $1 - \sigma$ errors on the plot. Therefore ξ was computed for all galaxies in bins of redshift between 0.3 and 1.0 with widths $\Delta z = 0.1$; from here a linear relationship for ξ as a function of redshift was derived: $\xi(z) = -0.9 \pm x(z) + 1.2 \pm y$. This correction was used to calculate the fraction of disks on the red sequence:

$$f_{D|R} = \frac{N_{RD} \times \xi^{-1}}{N_{RD} + N_{RE}} \quad (4)$$

4 RESULTS

In this section we present our results of the evolution of star-forming and quenched disc and elliptical galaxies from

$z = 1$ to $z = 0.2$ in a sample of 2x,xxx *COSMOS* galaxies morphologically classified in GZH. We show the evolution of each of the four types of populations as functions of redshift in four bins of stellar mass (Figure 7), and the fractions of red disks galaxies with respect to all disks, and to all red sequence galaxies (Figure 8).

In Figure 7 we plot the fractional contribution of blue/star-forming disks, blue/star-forming ellipticals, red/passive disks, and red/passive ellipticals vs. redshift in four stellar mass bins. For all masses, blue disks are the plurality population at each redshift. The red disk population is most abundant in the highest mass bin, and at fixed redshift their contribution decreases with mass. Red ellipticals tend to significantly outnumber red disks except in the highest mass/redshift bin, where they are in almost equal quantity. Blue ellipticals represent an insignificant fraction for galaxies with mass $\log(M/M_{\odot}) > 10.7$, but begin to outnumber the red disk population at lower masses.

Red disk galaxies are presumed to form primarily from blue disks galaxies which have quenched without undergoing a morphological transformation. If this is true, and if the resulting quenched disks do not continue in their evolution, one would expect a “pile up” of red disks as time progresses, resulting in an increasing fraction from right to left. This trend is observed in the two lowest mass bins, however there is no large change in fraction in the $M \sim 10.85$ bin, and even a small decrease in the highest mass bin. If we assume that red disks are continuously produced from blue disks, even

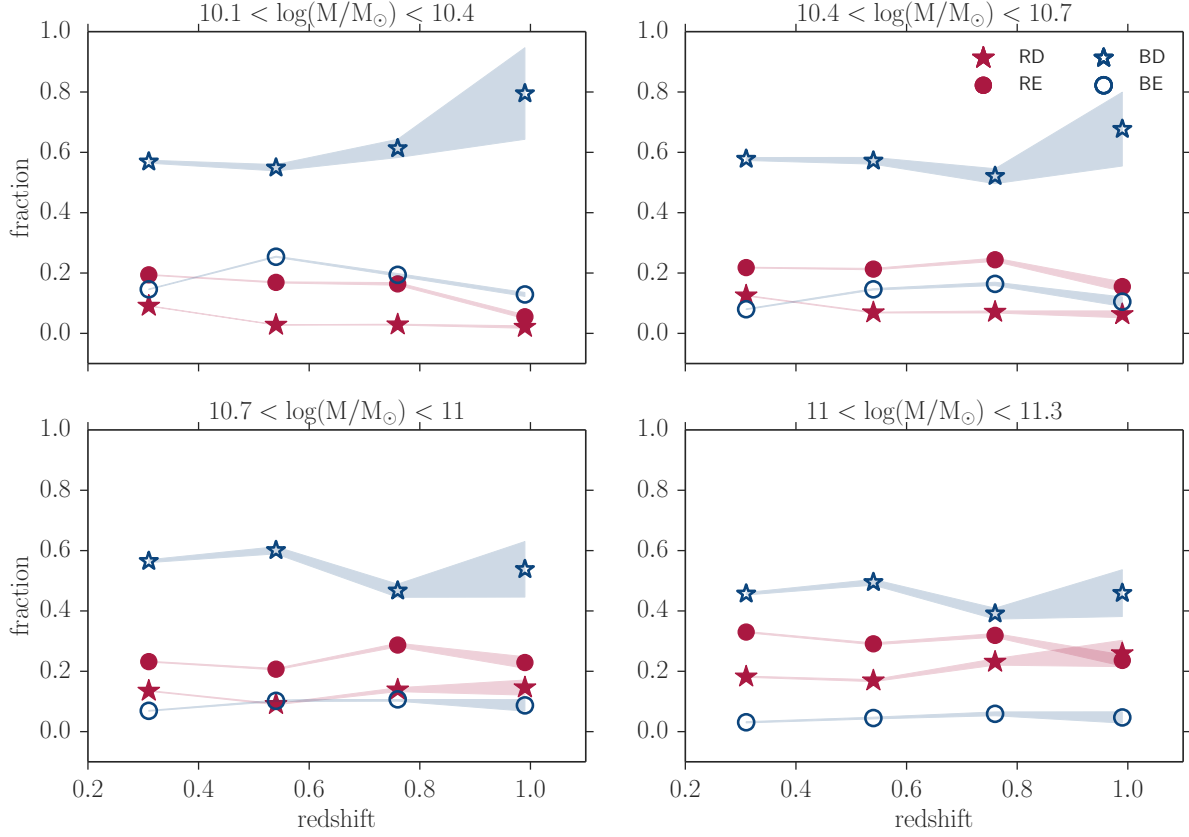


Figure 7. Evolution of four types of galaxy populations since $z = 1$: blue disks (blue open stars), red disks (red closed stars), blue ellipticals (blue open circles), and red ellipticals (red closed circles). Each point represents the fraction of the indicated type with respect to the total population, such that all points in a given redshift, mass bin sum to 1. Errors on each fraction are indicated by the shaded regions, and are propagations of \sqrt{N} counting errors and the errors associated with the functional fits to the correction terms ξ_{disk} and $\xi_{\text{elliptical}}$ (Section 3.2).

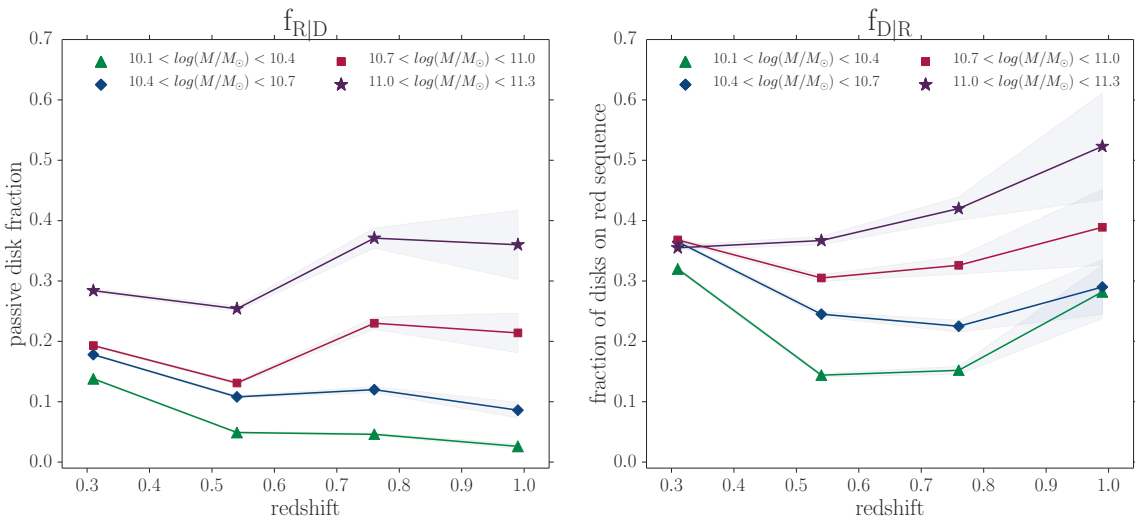


Figure 8. Left: Passive disk fraction ($N_{\text{red disks}}/(N_{\text{red disks}} + N_{\text{blue disks}})$) vs redshift in four mass bins. **Right:** Fraction of disks on the red sequence ($N_{\text{red disks}}/(N_{\text{red disks}} + N_{\text{red ellipticals}})$) vs redshift in four mass bins. Errors on each fraction are indicated by the shaded regions, and are propagations of \sqrt{N} counting errors and the errors associated with the functional fits to the correction terms ξ_{disk} and $\xi_{\text{elliptical}}$ (Section 3.2).

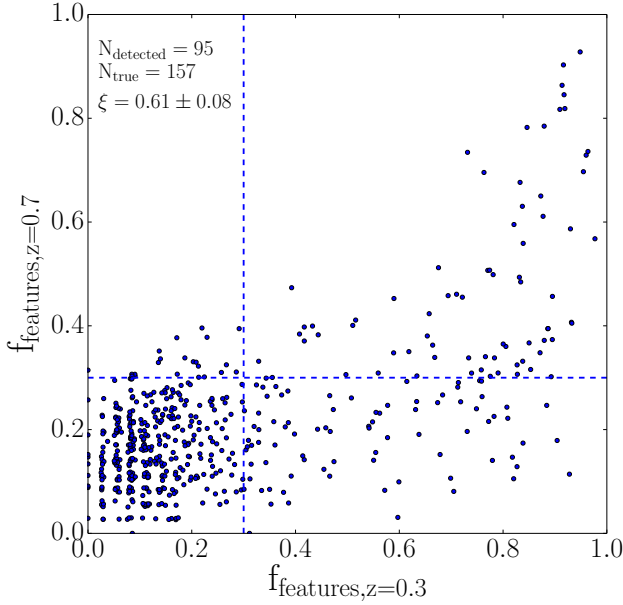


Figure 4. Example calculation of completeness ξ at redshift $z = 0.7$. Points represent FERENG12 images classified in Galaxy Zoo. The y-axis corresponds to the value of f_{features} measured at the galaxy redshifted to $z = 0.7$, and the x-axis corresponds to the value of f_{features} measured at the galaxy redshifted to $z = 0.3$. On average, the f_{features} is lower at the higher redshift, indicating users on average have more difficulty identifying features in images at higher redshifts. The dotted lines correspond to $f_{\text{features}}=0.3$, the threshold above which a galaxy is considered to have a disk. Galaxies to the right of the vertical dashed line were identified as disks at the lowest redshift $z = 0.3$, the total number defined as N_{true} , the true number of disks. Galaxies above the horizontal dash line were identified as disks at the higher redshift $z = 0.7$, the total number defined as N_{detected} . The ratio $\xi = N_{\text{detected}}/N_{\text{true}}$ is the completeness value; in this example, only 61% of disks were detected at $z = 0.7$.

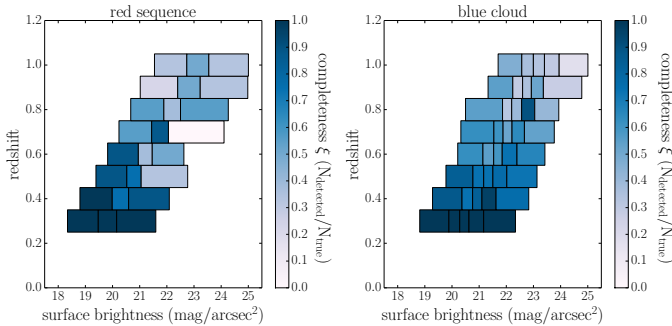


Figure 5. Completeness ξ as a function of redshift and surface brightness for red sequence (left) and blue cloud galaxies (right). In each redshift bin, galaxies were binned by surface brightness in varying widths such that $N_{\text{detected}} + N_{\text{true}} \geq 10$ in each bin. The completeness ξ was computed in each z, μ bin, represented by the colors. Darker colors represent a completeness of 1, such that all disks were detected, while fainter colors represent a completeness near 0, representing a failure to detect disks. ξ tends to decrease with redshift, but no correlation of ξ with surface brightness is observed at fixed redshift.

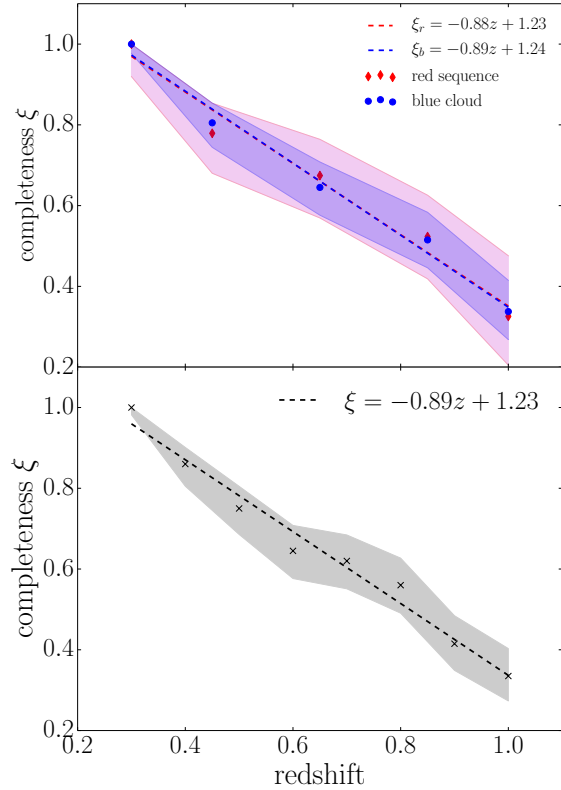


Figure 6. Top: Completeness ξ as a function of redshift for red sequence and blue cloud FERENG12 galaxies separately. Both populations show a strong dependence on ξ with redshift, but are indistinguishable from each other. **Bottom:** Completeness as a function of redshift for all FERENG12 galaxies (red and blue combined). The equation representing the linear fit is displayed.

at a small rate, then a constant or decreasing fraction can only be explained if their numbers are simultaneously being depleted, presumably by a morphological transformation to red elliptical.

The evolution of the red disk population is more apparent in Figure 8. On the left is the ratio of red disks to all disks ($f_{R|D} = N_{\text{red disks}}/(N_{\text{red disks}} + N_{\text{blue disks}})$), and the right shows the fraction of disks on the red sequence ($f_{D|R} = N_{\text{red disks}}/(N_{\text{red disks}} + N_{\text{red ellipticals}})$). In both fractions, there is a clear mass-dependence with the trends exhibited as functions of redshift. $f_{R|D}$ is constant for $M > 10.7$, and increases for the lower mass bins. An increase in $f_{R|D}$ could be driven by the increase of red disks or a depletion of blue disks; Figure 7 shows the increase may be driven more from the latter at $z \sim 1$, and the former at lower redshift. On the right, we find a decrease in $f_{D|R}$ for all masses in the interval from $z \sim 1$ to $z \sim 0.8$. Figure 7 shows that this is mainly driven by the increase in red ellipticals during this time, which is consistent with higher merger rates at this epoch (reference?). From $z \sim 0.8$ to $z \sim 0.3$, $f_{D|R}$ continues to decrease for galaxies $\log(M/M_{\odot}) > 11$, is constant for galaxies $\log(M/M_{\odot}) \sim 10.85$, and increases for the lower mass bins. From Figure 7, we confirm that the increase present in the low mass galaxies is driven more

by increases in the proportion of red disks, and not from a depletion of red ellipticals. The increase of $f_{R|D}$ and $f_{D|R}$ with redshift observed at low masses, coupled with the constant or decreasing trends for high masses, suggests that low mass red disk galaxies may be more likely to remain as such, while more massive red disk galaxies are more likely to further evolve via a morphological transformation.

The downward trend we observe in $f_{D|R}$ for massive galaxies is in agreement with Bundy et al. (2010) (hereafter B10) who perform a similar analysis of the morphological makeup of the red sequence. As suggested previously, a downward trend of $f_{D|R}$ represents either a depletion of the total pool of red disks (via a transformation to elliptical), but could also be an indication of an increase in the pool of red ellipticals (which could result from blue or red disks transforming morphology). In contrast, an upward trend is only possible via a pile-up of red disks, which is what we observe for the lower mass bins, and is in disagreement with B10. At the lowest redshift bin ($z \sim 0.3$), we measure similar absolute fractions of disks occupying the red sequence for all masses. However, B10 find their contribution to increase at higher lookback time to $z = 1$, while we find a decreasing contribution.

The fact that our results agree for the highest mass at all redshifts, but only at the lowest redshift for lower masses, suggests the differences may be attributed in biases in morphological classification. B10 identifies early and late-type disk galaxies using ZEST (Scarlata et al. 2007) morphologies, which they acknowledge are biased towards disk classification for faint apparent magnitudes, which tend to be attributed to the lowest mass, highest redshift objects. This bias could influence their observed increase in red sequence disks toward $z = 1$ for low masses. On the opposite end, GZ classifications tend to be biased towards elliptical morphologies at fainter magnitudes. We attempted to quantify and correct for this effect as described in Section 3.1, but if our correction was under-estimated, that may have driven the decreasing abundance of disk galaxies observed at increasing redshift for low masses. However, it has been shown in the local Universe that red disk galaxies tend to be more massive, as in Masters et al. (2011). If this is true at all epochs, we would not expect such a significant contribution of red disks for low mass galaxies as found in B10.

5 DISCUSSION

We have examined the evolution of red disk galaxies since $z = 1$ in Figures 7 and 8. The different trends observed in the abundance of red disks for different bins of mass are consistent with a physical scenerio in which 1) more massive galaxies are more likely to become passive disks (given by the higher proportion of red disks in the high mass bin of Figure 7), and 2) less massive galaxies who enter a red disk phase are more likely than massive galaxies to remain in that phase, rather than transform to elliptical (given by the increase of $f_{D|R}$ from $z = 1$ to $z = 0.3$ for low mass bins).

[reword. maybe phrase something as a question.] We now consider different mechanisms which could lead to a galaxy entering a red disk stage, and discuss whether each option would agree with the mass dependencies we've observed in the results.

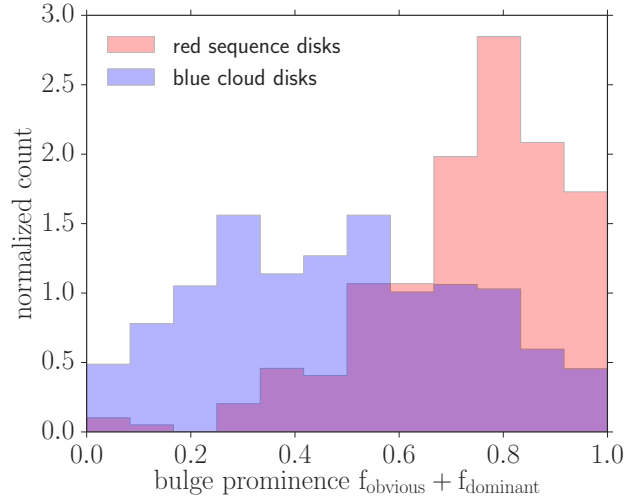


Figure 9. *yo*

What forms a passive disk, and why are they more common in massive galaxies? Why are more massive galaxies more likely to transition quickly out of this phase, while less massive galaxies remain in the phase?

5.1 Secular quenching of blue disks

Perhaps the most straight-forward mechanism by which a disk could quench without changing morphology is a purely secular process, in which the galaxy's gas supply is simply used up from continued star-formation. This scenario is unlikely to account for a significant portion of the creation of the red disk population, as the timescales for this type of quench would be 1-3Gyr, and galaxies are much more likely to have environmental interactions within that time.

5.2 Timescales

5.3 Disk regrowth

[put somewhere] Our first point is in agreement with literature which explores the unimodality of disk galaxies across a CMD (Schawinski et al. 2014; Powell et al. 2017). The smooth transition from the blue cloud to the red sequence in the distribution of low to medium mass disk galaxies is evidence for slow quenching timescales. For higher mass disk galaxies, the unimodality is broken, suggesting a more rapid quenching. This could be due to a higher merger rate for more massive galaxies, or as suggested by Schawinski et al. (2014), evidence for a mass-quenching effect, in which the galaxy's halo reaches a critical mass whereby the gas is inhibited from cooling sufficiently to continue star-formation (Kormendy & Kennicutt 2004; Dekel & Birnboim 2006; Peng et al. 2010). This result is also consistent with B10, who observe the strongest decrease in $f_{D|R}$ from $z = 1$ to $z = 0.3$ for their most massive galaxies.

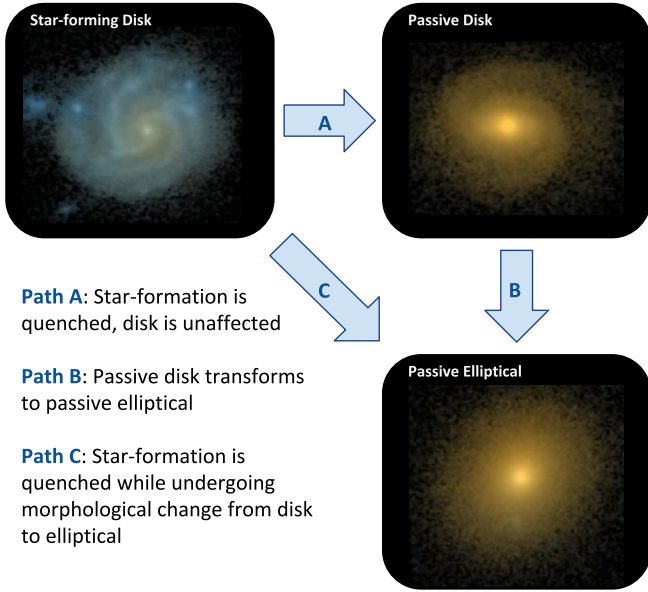


Figure 10. Cartoon representing three common evolutionary pathways of star-forming disk galaxies. Path A represents an active star-forming galaxy which quenches without destroying the disk, becoming a red disk. Path B represents a red disk morphologically transition to red elliptical. Path C represents a blue disks simultaneously quenching and morphologically transforming to become a red elliptical.

6 CONCLUSIONS

We have investigated the influence of the passive disk population by measuring the relative abundances of blue disks, red disks, and red ellipticals since $z = 1$ using morphological classifications from Galaxy Zoo: Hubble and rest-frame colors from UltraVISTA. Using data from artificially-redshifted FERENGI2 images to quantify the known redshift bias in the GZ classifications, we implemented a correction to the incompleteness in the number of disks detected as a function of redshift. The relative numbers were measured in terms of the fraction of disk galaxies that are red $f_{R|D}$ and the fraction of disk galaxies on the red sequence $f_{D|R}$. Our main conclusions are as follows:

- $f_{R|D}$ and $f_{D|R}$ decrease from $z = 1$ to $z = 0.3$ for massive galaxies, and increase for the least massive galaxies.
- Low mass galaxies which experience a passive disk phase are more likely than massive galaxies to remain disks, while massive galaxies are more likely to continue their evolution by transforming to passive ellipticals. To quantify and validate this result would require the implementation of a semi-analytic model.

The data in this paper are the result of the efforts of the Galaxy Zoo Hubble volunteers, without whom none of this work would be possible. Their efforts are individually acknowledged at authors.galaxyzoo.org. Please contact the author(s) to request access to research materials discussed in this paper.

MG, CS, MB, and LF gratefully acknowledge support from the US National Science Foundation Grant AST1413610.

This publication makes use of data products from the Two Micron All Sky Survey, which is a joint project of the University of Massachusetts and the Infrared Processing and Analysis Center/California Institute of Technology, funded by the National Aeronautics and Space Administration and the National Science Foundation.

This project made heavy use of the Astropy packages in Python (Robitaille et al. 2013), the *seaborn* plotting package (Waskom et al. 2015), and the Tool for OPERations on Catalogues And Tables (TOPCAT), which can be found at www.starlink.ac.uk/topcat/ (Taylor 2005).

Funding for the SDSS and SDSS-II has been provided by the Alfred P. Sloan Foundation, the Participating Institutions, the National Science Foundation, the U.S. Department of Energy, the National Aeronautics and Space Administration, the Japanese Monbukagakusho, the Max Planck Society, and the Higher Education Funding Council for England. The SDSS website is <http://www.sdss.org/>.

The SDSS is managed by the Astrophysical Research Consortium for the Participating Institutions. The Participating Institutions are the American Museum of Natural History, Astrophysical Institute Potsdam, University of Basel, University of Cambridge, Case Western Reserve University, University of Chicago, Drexel University, Fermilab, the Institute for Advanced Study, the Japan Participation Group, Johns Hopkins University, the Joint Institute for Nuclear Astrophysics, the Kavli Institute for Particle Astrophysics and Cosmology, the Korean Scientist Group, the Chinese Academy of Sciences (LAMOST), Los Alamos National Laboratory, the Max-Planck-Institute for Astronomy (MPIA), the Max-Planck-Institute for Astrophysics (MPA), New Mexico State University, Ohio State University, University of Pittsburgh, University of Portsmouth, Princeton University, the United States Naval Observatory and the University of Washington.

REFERENCES

- Ann H. B., Thakur P., 2005, *The Astrophysical Journal*, 620, 197
- Arnouts S. et al., 2007, *Astronomy and Astrophysics*, 476, 137
- Athanassoula E., 1992, *Monthly Notices of the Royal Astronomical Society*, 259, 328
- Baldry I. K., Glazebrook K., Brinkmann J., Ivezić Ž., Lupton R. H., Nichol R. C., Szalay A. S., 2004, *The Astrophysical Journal*, 600, 681
- Barden M., Jahnke K., Häußler B., 2008, *The Astrophysical Journal Supplement Series*, 175, 105
- Bekki K., Couch W. J., Shioya Y., 2002, *The Astrophysical Journal*, 577, 651
- Bell E. F. et al., 2004, *The Astrophysical Journal*, 608, 752
- Brinchmann J., Charlot S., White S. D. M., Tremonti C., Kauffmann G., Heckman T., Brinkmann J., 2004, *Monthly Notices of the Royal Astronomical Society*, 351, 1151
- Bruzual & Charlot, 2003, *Monthly Notices of the Royal Astronomical Society*, 344, 1000
- Bundy K. et al., 2010, *The Astrophysical Journal*, 719, 1969
- Cassata P. et al., 2008, *Astronomy and Astrophysics*, 483, L39

- Cirasuolo M. et al., 2007, *Monthly Notices of the Royal Astronomical Society*, 380, 585
- Correa C. A., Schaye J., Clauwens B., Bower R. G., Crain R. A., Schaller M., Theuns T., Thob A. C. R., 2017
- De Lucia G., Springel V., White S. D. M., Croton D., Kauffmann G., 2006, *Monthly Notices of the Royal Astronomical Society*, 366, 499
- Dekel A., Birnboim Y., 2006, *Monthly Notices of the Royal Astronomical Society*, 368, 2
- Deng X.-F., He J.-Z., Wu P., Ding Y.-P., 2009, *The Astrophysical Journal*, 699, 948
- Devour B., Bell E., 2017, 5
- Dressler A., Smail I., Poggianti B. M., Butcher H., Couch W. J., Ellis R. S., Oemler, Jr. A., 1999, *The Astrophysical Journal Supplement Series*, 122, 51
- Franzetti P. et al., 2007, *Astronomy and Astrophysics*, 465, 711
- Friedli D., Benz W., 1993, *Astronomy and Astrophysics*, 268
- Galloway M. A. et al., 2015, *Monthly Notices of the Royal Astronomical Society*, 448, 3442
- Giallongo E., Salimbeni S., Menci N., Zamorani G., Fontana A., Dickinson M., Cristiani S., Pozzetti L., 2005, *The Astrophysical Journal*, 622, 116
- Goto T. et al., 2003, *Publications of the Astronomical Society of Japan*, 55, 757
- Governato F. et al., 2009, *Monthly Notices of the Royal Astronomical Society*, 398, 312
- Gunn J., E. and Gott, III J., 1972, *apj*, 176, 1
- Hawarden T. G., Mountain C. M., Leggett S. K., Puxley P. J., 1986, *Monthly Notices of the Royal Astronomical Society*, 221, 41P
- Ho L. C., Filippenko A. V., Sargent W. L. W., 1997
- Hughes T. M., Cortese L., 2009, *Monthly Notices of the Royal Astronomical Society: Letters*, 396, L41
- Ilbert O. et al., 2013, *Astronomy & Astrophysics*, 556, A55
- Kauffmann G. et al., 2003, *Monthly Notices of the Royal Astronomical Society*, 341, 54
- Kormendy J., Kennicutt R. C., 2004, *Annual Review of Astronomy and Astrophysics*, 42, 603
- Larson, R.B., Tinsley, B.M. and Caldwell C., 1980, *The Astrophysical Journal*, 237, 692
- Lilly S. et al., 1998, *The Astrophysical Journal*, 500, 75
- Loveday J. et al., 2011
- Martin D. C. et al., 2005, *The Astrophysical Journal*, 619, L1
- Martin D. C. et al., 2007, *The Astrophysical Journal Supplement Series*, 173, 342
- Masters K. L. et al., 2010, *Monthly Notices of the Royal Astronomical Society*, 405, 783
- Masters K. L. et al., 2011, *Monthly Notices of the Royal Astronomical Society*, 411, 2026
- McCracken H. J. et al., 2012, *Astronomy & Astrophysics*, 544, A156
- Mignoli M. et al., 2009, *Astronomy and Astrophysics*, 493, 39
- Moran S. M., Ellis R. S., Treu T., Salim S., Rich R. M., Smith G. P., Kneib J.-P., 2006, *The Astrophysical Journal*, 641, L97
- Morselli L., Renzini A., Popesso P., Erfanianfar G., 2016, *Monthly Notices of the Royal Astronomical Society*, 462, 2355
- Negroponte J., White S. D. M., 1983, *Monthly Notices of the Royal Astronomical Society*, 205, 1009
- Peng Y., Maiolino R., Cochrane R., 2015, *Nature*, 521, 192
- Peng Y.-j. et al., 2010, *The Astrophysical Journal*, 721, 193
- Planck Collaboration et al., 2015
- Poggianti B. M., Smail I., Dressler A., Couch W. J., Barger A. J., Butcher H., Ellis R. S., Oemler, Jr. A., 1999, *The Astrophysical Journal*, 518, 576
- Powell M. C., Urry C. M., Cardamone C. N., Simmons B. D., Schawinski K., Young S., Kawakatsu M., 2017, *The Astrophysical Journal*, 835, 22
- Quilis V., Moore B., Bower R., 2000, *Science*, 288, 1617
- Robertson B., Bullock J. S., Cox T. J., Di Matteo T., Hernquist L., Springel V., Yoshida N., 2006, *The Astrophysical Journal*, 645, 986
- Robitaille T. P. et al., 2013, *Astronomy & Astrophysics*, 558, A33
- Salim S. et al., 2005, *The Astrophysical Journal*, 619, L39
- Scarlata C. et al., 2007, *The Astrophysical Journal Supplement Series*, 172, 406
- Schawinski K. et al., 2014, 21
- Scoville N. et al., 2007, in *AIP Conference Proceedings*, Vol. 943, AIP, pp. 221–228
- Sellwood J. A., Wilkinson A., 1993, *Reports on Progress in Physics*, 56, 173
- Shlosman I., Frank J., Begelman M. C., 1989, *Nature*, 338, 45
- Skrutskie M. F. et al., 2006, *The Astronomical Journal*, 131, 1163
- Sparre M., Springel V., 2016, 12
- Springel V., Di Matteo T., Hernquist L., 2005, *The Astrophysical Journal*, 620, L79
- Springel V., Hernquist L., 2005, *The Astrophysical Journal*, 622, L9
- Steinhauser D., Schindler S., Springel V., 2016
- Strateva I. et al., 2001, *The Astronomical Journal*, 122, 1861
- Taylor M. B., 2005, in *Astronomical Society of the Pacific Conference Series*, Vol. 347, p. 29
- van den Bergh S., 1976, *The Astrophysical Journal*, 206, 883
- van Dokkum P. G. et al., 2006, *The Astrophysical Journal*, 638, L59
- Waskom M. et al., 2015
- Willett K. W. et al., 2016, 32
- Wyder T. K. et al., 2007